TRACERS IN PHYSIOLOGICAL SYSTEMS MODELING

Joseph C. Anderson and James B. Bassingthwaighte

Department of Bioengineering

University of Washington

Seattle, WA 98195 - 5061

Running Head: Principled Physiological Modeling (#737)

Address for Correspondence:

James B. Bassingthwaighte, M.D., Ph.D.

University of Washington, Box 355061

Dept. of Bioengineering

Seattle, WA 98195-5061

Phone: 206-685-2005 and FAX 206-685-3300

Email: jbb2@u.washington.edu

Published as:

615. Anderson JC and Bassingthwaighte JB. Tracers in physiological systems modeling. In: Mathematical Modeling in Nutrition and Agriculture. Proc 9th Internat Conf on Mathematical Modeling in Nutrition, Roanoke, VA, August 14-17, 2006, edited by Mark D. Hanigan JN and Casey L Marsteller. Virginia Polytechnic Institute and State University, Blacksburg, VA, 2007, pp 125-159.

Abstract

Metabolic events within cells are intimately linked with the external influences of substrate delivery and metabolite removal. These influences include the level of cellular activity, the local blood flow, transmembrane transport rates, and humoral and neural regulation of receptors and reaction rates. The question “What are the basic principles that the developers of tracer models should use?” evokes discussion on the scope of the modeling: an extremes is “minimal modeling”, wherein one considers only the observations of the injected tracer-labelled solute itself (as in pharmacokinetics), its reaction products, or extend to its effects on the physiology (as in pharmacodynamics). Minimal modeling can work for classification or diagnosis but, unless the model has the depth to encompass mechanisms of tracer handling, doesn’t often provide an explanation. Here we advocate adherence to a broad set of principles for the design and application of models to the understanding of physiological systems: (1) consider the anatomy (a biological constraint) as an essential part of the data, (2) take into account the background physiological state of the subject (biochemical, thermodynamic constraints), (3) consider the processes that the tracer labelled solutes undergo (mechanisms of transport and reaction), (4) be obedient to the laws of physics and chemistry (conservation principles for mass, energy, charge, momentum, etc.), and (5) adhere to a set of modeling standards allowing reproducibility and dissemination of the model. A two compartment model with a binding site illustrates that recognition of the anatomic constraints would foster a better understanding of the system kinetics. Another example is to abandon the lumped compartmental representation of spatially extended capillary-tissue exchange in favor of using anatomic-based equations, thereby obtaining physically meaningful esxtimates of parameter values.

Key Words: tracer, tracee, metabolic physiologic modeling, lumped compartmental versus spatially distributed systems, capillary-tissue exchange, membrane transporters, enzyme reactions, steady state versus transient states.

INTRODUCTION

Advances in computational speed and simulation interface technology now make it practical to choose valid physiological modeling approaches rather than using minimal models for classification or description. Here we will argue that by following a few general guidelines and standard scientific ideas one can bring additional power, reliability, and accuracy in parameterization, and, best of all, improved insight into the processes involving solute transport.

The "principles" are a combination of scientific principles and psychological aids or perspectives that make it easier to keep on the straight and narrow. Here we address particularly the users of "compartmental analysis" for it appears that the nomenclature and computational toolkits commonly used are compromising the efficacy of this particular community of skilled scholars in determining mechanisms to explain the observed kinetics. This is in spite of the fact that Berman (1963) in his classic article on modeling clearly espoused properly principled modeling, including examination of underlying assumptions. While making this bold general criticism, we recognize that there is an immense amount of productive contributory work accomplished with the same tool kit that we are criticizing. At the same time, we suggest using an alternative methodology that forces adherence to scientific principles and facilitates placing particular tracer models into the context of discovery science, specifically, to attempt to elucidate biological mechanisms in networks of processes, going beyond the kinetics.

Integrative modeling is only beginning. Each of the thousands of models in existence is potentially a component module in a larger scale integrated model. Model archiving and public accessibility will make it possible for future investigators to combine modules, thereby constraining the behavior of the individual components. It is therefore contributory to the community effort to make each model available, understandable, reproducible, verifiable and to provide along with it the data that demonstrates its validity with respect to the biology.

The primary recommendations for the modeling of biological systems are:

1. **Use the known anatomy, structure, and composition to constrain estimates** of local and overall volumes of distribution, routes of transport, and other kinetic possibilities. These are not necessarily measured in every experiment, but in general should be considered as parts of the experimental data since their means and standard deviations are known and they provide realistic constraints. For example, the water fraction of heart muscle is so narrowly constrained that it can be used as a constant, being 0.78 +/- 0.01 ml/g tissue (Yipintsoi et al 1972).
2. **Define parameters and variables in physiologically meaningful terms** in order to stimulate re-examination of assumptions at each stage. Consider the details of the underlying physiology in defining the model in order to constrain its form and behavior. For example, use continuity in concentration profiles along segments of the vascular system or within cells. In using mathematics that describes the biology, don't compromise the mathematics to fit limitations in computational methods, but compromise later, with caution. Use standardized terminology where possible, and try to use terms defined in ontologies such as the Foundations of Medical Anatomy in order to maintain uniqueness of terms.
3. **Apply conservation principles (mass, charge, volume, energy)**, and relevance to a viable steady state, preferably checking for these in each program. Provide thermodynamic constraints on all reactions. ΔG counts. Use units in defining all variable and parameters. Use

technology which uses automatic unit balance checking in order to force identification of errors.

4. Recognize that **the fundamental description of the kinetics of tracers is always at the molecular level,** therefore "think like a molecule" on how each process occurs: Convected in in the blood in a bound or free state? How is the membrane traversed? How does each reaction occur, and where? The tenet of tracer methods is not that the system should be in steady state, but that the linearized coefficients for the tracer kinetics are slaved to the fluxes for the mother substance in both transient and steady states. Use dual models, mother and tracer, where the mother model, for tracee, contains all the physiological mechanisms, while the tracer model has its coefficients directly derived from the current ambient state for tracee.
5. **Adhere to standard requirements** for the design, performance, documentation, and dissemination of models. The goal in presenting a model is easy and accurate reproducibility by a user community of researchers, teachers, and students. Check lists for documenting and archiving a model are being developed, and a preliminary version can be found at www.physiome.org/Models/standards.html. Whenever such standards are not being met, think of of it as an invitation to explain that something is missing or assumed in the modeling. It probably will not be long before journals establish such criteria for publication. Certainly the federal funding agencies are moving rapidly toward requiring that the results of federally funded research be made publicly available.

Most commonly, the kinetics of exchange and metabolism are based on the idea that a solute (drug, substrate or metabolite, receptor, enzyme, etc.) can be treated as being within a lumped system, i.e. one wherein the concentration of the solute is everywhere uniform. "Lumped", "compartmental", or "stirred tank" representation allows the system to be described using ordinary differential equations, which is simpler than accounting for spatial gradients and using partial differential equations (PDEs). In this essay we argue that using PDEs is as simple conceptually as using ODEs, that modern simulation systems analysis tools makes PDE usage in practice as easy as using ODEs, and that the PDEs are required to obtain physically correct measures of parameters of many systems. The argument is simple: the use of incorrect representation of the anatomy of the system causes artifactual errors in parameter estimates for transport rates and reaction rates.

Such errors have been obvious to those examining oxygen exchange for a long time, since Krogh and Erlang (1919) modeled oxygen profiles in capillary tissue exchange units. They showed that if the tissue oxygen consumption was uniform there were nearly exponential gradients in oxygen tension, P_{O2}, along the capillary length, and parabolic profiles in P_{O2} in the tissue between capillaries. In blood-perfused tissues the calculation of the profiles is more complex because of the binding of oxygen to hemoglobin, Hb, and the influences of carbon dioxide, pH, and temperature, all of which have intracapillary gradients, on the oxygen binding. Axial gradients in P_{O2} are more linear than exponential (Dash and Bassingthwaighte, 2006). The fact that most drugs and hormones are also bound to blood components, e.g. retinone, fatty acids, either RBC or plasma proteins invites consideration of the similarity between the mechanisms of their exchanges and those of oxygen. Further, most drugs and solutes of interest are less soluble in membranes than is oxygen (whose transport across lipid membrane is so fast as to be limited solely by delivery to the membrane surface, not by the permeation process itself), and commonly require specialized transporters to facilitate transfer. Where transporters are required, there is virtually always competition for the binding sites, so transport rates for a foreign drug or a

tracer-labeled solute can be expected to be somewhat dependent on the ambient concentrations of those native solutes or other drugs.

One of the reasons for assuming stirred tank representation (compartmental models) was to reduce computation time, a goal rendered less critical with fast modern computers, but important when one has to optimize model predictions to fit many data sets. Modeling analysis for data on ^{15}O-oxygen from positron emission tomography (PET) was particularly slow because it required not only iteration but also required solving a steady state model for non-tracer oxygen (Li et al 1997) as well as the tracer data. To speed up this computation, Dash and Bassingthwaighte (Ann Biomed Eng 32: 1767-1793, 2004) developed invertible Hill-type saturation expressions for hemoglobin (Hb) saturations and blood-tissue gas exchanges accounting for the simultaneous hemoglobin binding of O_2, CO_2, H^+, 2,3-DPG, and the effects of temperature. The equations allow rapid calculation of the redistribution that occurs along the length of capillary-tissue exchange regions in the lung or in tissue. Likewise these equations can be used to account for pH buffering in the blood, and for exchanges of gases in the capillaries of tissues and lungs in a whole body model describing gas exchange. A prototype of a circulatory-respiratory exchange model is available at www.physiome.org/Models. This approach, implementing fast algorithms, is only one of many tricks that one can use to save time.

Other approaches involve a reduction in the number of free parameters in an optimization procedure, such as using known values for volumes of distribution or known K_m's for enzymatic reactions or transporters. Additional efficiency is gained by using thermodynamic constraints (e.g., Haldane) to limit parameter ranges and thus shrink the available state space. Using the known equilibrium constants in biochemical systems analysis, e.g. in flux balance analysis, reduces the range of individual flux estimates in E.coli metabolism by about 2 orders of magnitude (Beard, Liang, Qian BJ, 2002).

APPROACHES AND METHODS

Definition of tracer, C*:

The advantage of using tracers is that nonlinear processes are rendered linear when the overall system is in steady state for all solutes except the tracer itself. The rationale for this is that the concentration of the tracer-labeled solute C* is in negligible concentration compared to that of the non-tracer mother substance, C, so that changes in C* has no impact on the kinetics for the mother substance:

For the transport of C, the rate constant depends on its concentration *C*, for example, relative to the dissociation constant for the process of binding to the transporter:

$$dC/dt = -k(C) \cdot C \ , \qquad (1)$$

where *C* is a concentration, M, $k(C)$ is a transfer or reaction rate, s^{-1}, which is a function of the concentration of *C*. When tracer (C*) is transported by the same process as the mother substance, then the transport of *C* + *C** is essentially the same as that for *C* alone and the transport of *C** is given by

$$dC^*/dt = -k(C + C^*) \cdot C^*. \quad (2)$$

By definition, tracer concentrations are $C^*/C << 1$ and usually $< 1/10^{12}$. As a result, $k(C+C^*) = k(C)$ and $k(C)$ is independent of C^*, and

$$dC^*/dt = -k(C) \cdot C^*, \quad (3)$$

showing that the rate constant for C^* is identical to that for the mother substance C, at the particular concentration, C, in steady state. When the concentration of C is slowly varying then the same considerations apply, but in that case $k(C)$ becomes $k(C(t))$. Likewise, when C varies spatially within a capillary-tissue exchange region, *i.e.*, $C(x,t)$ is a function of position x, then this rate is expressed as $k(C(x,t))$.

Writing dual models for tracee and tracer together:

Most tracer models are developed from node/edge relationships in networks of reacting species and then written in the form of linear sets of ordinary differential equations. This methodology is based on two independent assumptions: (a) that a node represents a time-dependent variable that is spatially uniform, as if concentrations are instantaneously mixed over a finite space, the compartment, and (b) that the edges, the rate processes, have linear, constant coefficients for tracer because the mother or tracee system is in a constant, non-oscillating steady state. We will explore the effects of deviations from these assumed conditions.

When (b) is applicable, then the rate coefficients for tracer can be considered linear and constant at each location in the system, though they are necessarily different in each location whenever the concentration of mother substance is different. A reliable way to approach the analysis of such a system is to model tracee and tracer together before jumping to the linearized tracer equations.

As a first example, to make the assumptions clear, we discuss a two compartment system, first for mother substance, tracee, and then for tracer. The second example will be a flow-through system, considering it as comprised of blood and tissue.

MODELING OF A TWO-COMPARTMENT SYSTEM

This section focuses on the effects of solute binding on volumes of distribution, on exchange rates and times to equilibration, and on the estimation of physiological parameters.

Model 1: Binding site in compartment 1 of a 2-compartment system, Non-tracer

Model 1A: Non-instantaneous binding (equivalent to a 3 compartment system)

This system is diagrammed in Figure 1. For this system the equations are:

$$dC_1/dt = -\frac{PS}{V_1}(C_1 - C_2) - k_{ON} \cdot B \cdot C_1 + k_{OFF} \cdot CB, \quad (4)$$

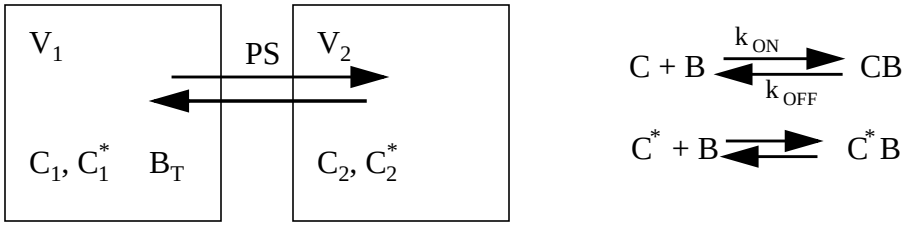

Figure 1: A two compartment system for the passive exchange of solute C between the stirred tanks. In tank 1 the solute may bind with a ligand B whose total concentration is B_T, mM, in accord with the reaction shown at right. The reaction rates for tracer C* are determined by the concentration C of tracee or mother solute. PS, ml/s, is a conductance, the permeability-surface area product of the membrane separating the two chambers, allowing bidirectional passive flux.

$$dCB/dt = k_{ON} \cdot B \cdot C_1 - k_{OFF} \cdot CB, \tag{5}$$

$$B = B_T - CB, \tag{6}$$

$$dC_2/dt = \frac{PS}{V_2}(C_1 - C_2). \tag{7}$$

where C is concentration of tracee, mM; t is time, seconds; PS is a passive conductance, a permeability-surface area product, cm/sec times cm^2, or ml/sec; V_1, ml, is the volume of compartment 1; k_{ON}, $mM^{-1}\ s^{-1}$, is the rate of binding of C to the ligand B within compartment 1 to form CB, and k_{OFF}, s^{-1}, is the rate of release of C from CB, so the dissociation constant,

$K_D = k_{OFF}/k_{ON}$, mM,

and B_T, mM, is the total concentration of ligand (bound + free); C_2, mM, is the concentration in compartment 2 whose volume is V_2, ml.

To illustrate the behavior of this model, B_T = 1 mM, K_D = 0.1 mM and solute is introduced into the system at an initial value of C_1=1 mM. The results are shown in Figure 2 for various values of k_{ON}. Because binding is slow relative to permeation, there is a rapid early overshoot in C_2 and a slow return to the final equilibrium condition where K_D =B*C_1/CB.

Model 1B: Instantaneous binding of solute to ligand in Compartment 1:

This is a reduced form of Model 1A assuming that the binding of C to any free B occurs instantaneously. When both k_{OFF} and k_{ON} are rapid CB can be calculated algebraically instead of using a differential equation. Using Eq. 5 and setting the derivative to zero to represent the equilibrium between C and CB, then

$$dCB/dt = 0 = k_{ON} \cdot B \cdot C_1 - k_{OFF} \cdot CB, \text{ and} \tag{8}$$

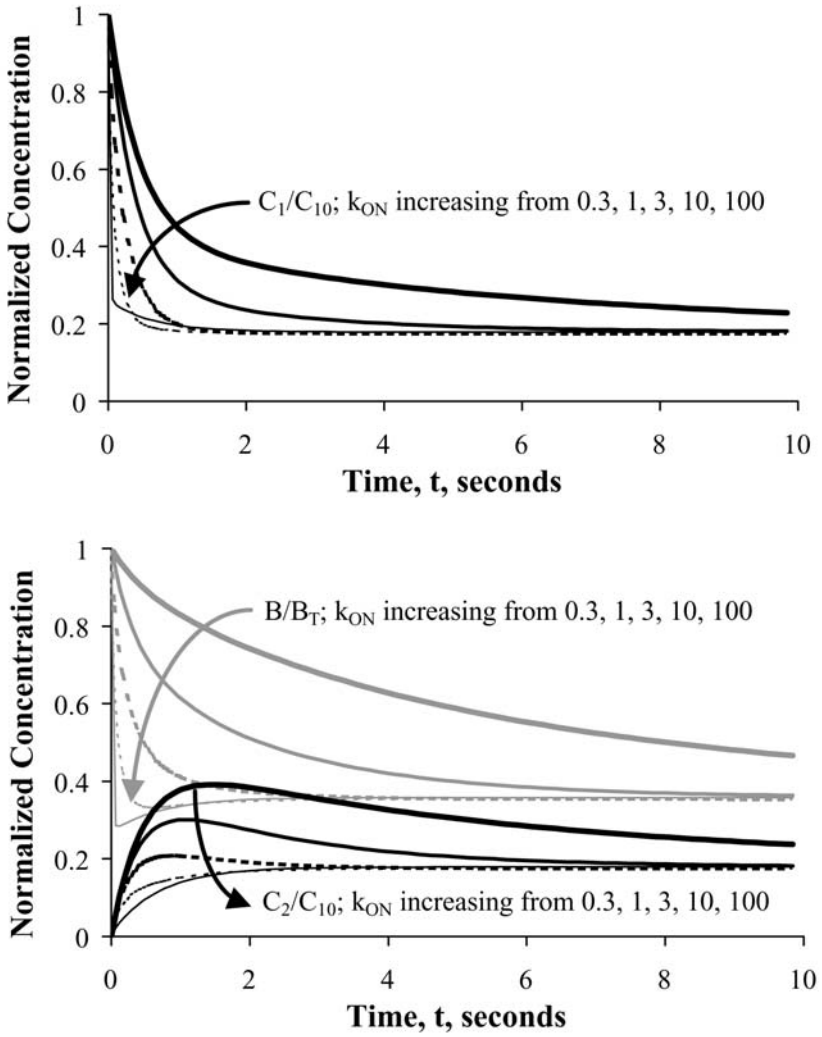

Figure 2: Equilibration of C across a barrier with a binding ligand in V_1. for increasing values of k_{ON} from 0.3 to 100 $mM^{-1}s^{-1}$. *Top panel:* The initial concentration C_1 was as if 1 μmole of C were injected in a volume V_1 of 1 ml at t = 0. Parameters were PS = 1 ml/s, B_T = 1 mM, K_D is constant at 0.1 mM, and V_2 = 1 ml. *Bottom panel:* Concentrations of free binding sites, B, and of C_2.

$$K_D = \frac{k_{OFF}}{k_{ON}} = \frac{B \cdot C_1}{CB}, \text{ and} \tag{9}$$

$$\frac{d(C_1 + CB)}{dt} = -\frac{PS}{V_1} \cdot (C_1 - C_2) \tag{10}$$

CB is defined by substitution of Eq. 6 into Eq. 9: $CB = (B \cdot C_1)/K_D = ((B_T - CB) \cdot C_1)/K_D$.

Solving for CB by rearranging the expression above gives an algebraic expression for CB independent of free B:

$$CB = \frac{B_T \cdot C_1}{K_D + C_1} \tag{11}$$

The equilibrium relationship between CB and C_1 can be substituted into Eq. 10 and after differentiation gives.

$$\frac{dC_1}{dt}\left(1 + \frac{B_T}{K_D + C_1} - \frac{B_T}{(K_D + C_1)^2}\right) = -\frac{PS}{V_1} \cdot (C_1 - C_2). \tag{12}$$

Now it can be seen that the theoretical volume of distribution is not V_1 but a larger volume, V_1^p . I The quadratic term is not relevant when C_1 is constant. Then, V_1^p can be seen to be a concentration-dependent volume of distribution at equilibrium:

$$V_1^p = V_1\left(1 + \frac{B_T}{K_D + C_1}\right), \tag{13}$$

At equilibrium, the effective volume of distribution, V_1^p or V_d, is defined by the actual concentration *CB* from Eq. 11 , which augments the free concentration

$$V_d = V_1(1 + CB/C_1) \tag{14}$$

Now Eq. 12 can be rewritten:

$$\frac{dC_1}{dt} = -\frac{PS}{V_1^p} \cdot (C_1 - C_2) \tag{15}$$

Now the system equations define C_1 by Eq. 15 (with Eq. 13), C_2 by Eq. 7 (unchanged), and 2-compartments using a modified, concentration-dependent volume of distribution. Plotting V_1^p versus C_1 (Figure 3) shows that the maximum V_1^p is at any $C_1 < K_D$ where most of the solute is bound and is $V_1(1 + B_T/K_D)$. When $C_1 = K_D$, half of B_T is bound and $CB = B$. At high concentrations much greater than K_D, all the binding sites are filled and V_1^p goes to V_1.

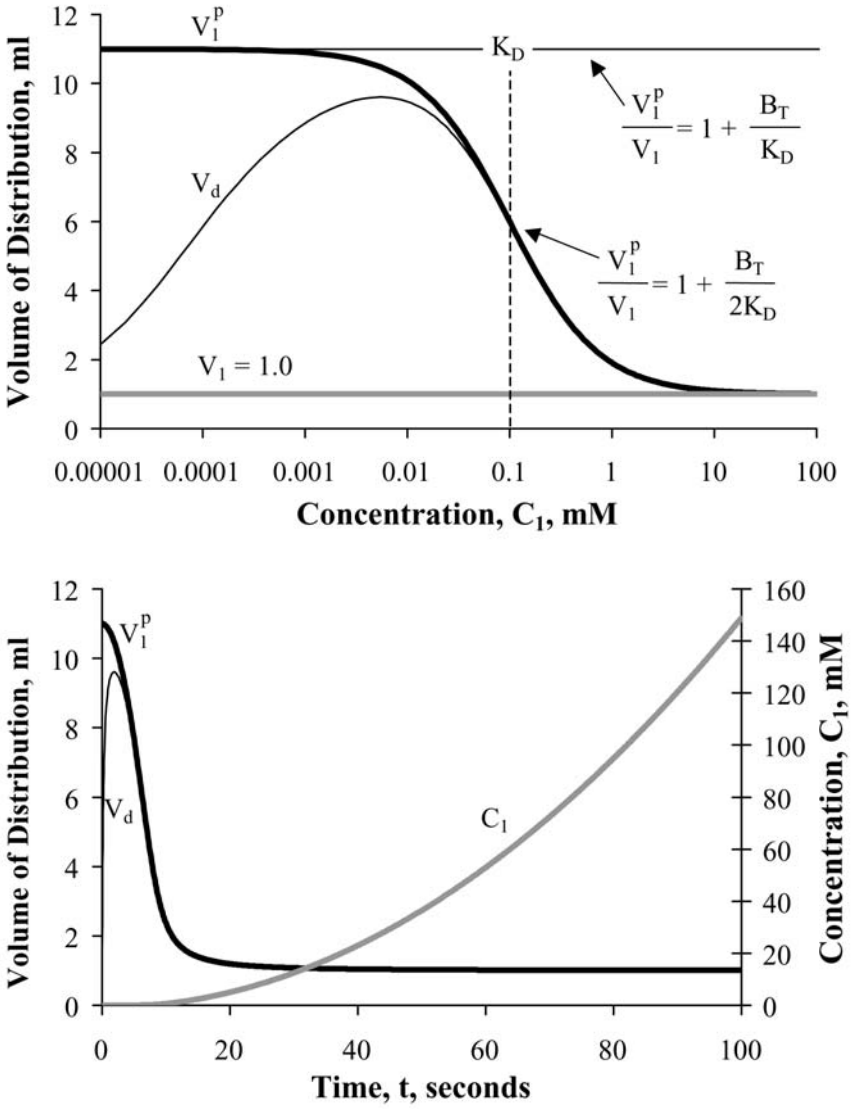

Figure 3: *Top panel*. Volumes of distribution, V_1^p (Eq13) for equilibrium binding and V_d (Eq14) for an unsteady state of increasing C_1 versus concentration C_1. *Bottom panel*. The *in silico* experiment was to raise the concentration C_1 at an accelerating rate into a stirred tank of volume V_1=1.0 ml (upper panel). Conditions were: K_D = 0.1 mM; k_{ON} = 100 $mM^{-1}s^{-1}$; and PS = 0. The rate of concentration increase in V_1 was 30 nM/s^2, such that after 20 seconds C_1 has reached 5 mM. The theoretical V_1^p (thick black line) can be seen to diminish in accord with Eq. 13 as C_1 rises. The actual or effective $V_d = V_1(1 + CB/C_1)$. V_d is initially equal to V_1 because CB is zero. Then CB rises rapidly as binding occurs to form CB, but in spite of the fairly high k_{ON} does not reach the equilibrium binding level V_1^p until about 5 seconds have passed at which point $V_d = V_1^p$.

In this example with B_T/K_D = 10, the maximum volume of distribution V_1^p is 11, and is observed when equilibrium is attained at low concentrations. However, when the solute does not arrive at the binding site instantly or does not react instantaneously, the effective volume of distribution V_d must be less, as shown by the thin black curve in Figure 3. Even when the binding rate is moderately high, k_{ON} = 100 $mM^{-1}s^{-1}$, a lag in the effective volume of distribution is present when C_1 is rising (bottom panel of Figure 3). During this transient, the maximum V_d is less than that expected theoretically, V_1^p .

Model 1.C: Tracer added to a slow binding system in equilibrium for non-tracer.

The phrase slow binding (and slow release) implies that k's are similar to PS/V_1^p . Tracer concentrations are C_1^* and C_2^*. The tracer equations take their coefficients from the tracee, and the equations are the same as for tracee, Eqs. 4 to Eq. 7:

$$dC_1^*/dt = -\frac{PS}{V_1}(C_1^* - C_2^*) - k_{ON} \cdot B \cdot C_1^* + k_{OFF} \cdot C^*B, \quad (16)$$

$$dC^*B/dt = k_{ON} \cdot B \cdot C_1^* - k_{OFF} \cdot C^*B, \quad (17)$$

$$B = B_T - CB - C^*B, \text{ and} \quad (18)$$

$$dC_2^*/dt = \frac{PS}{V_2}(C_1^* - C_2^*) \quad (19)$$

where Eq. 18 for free B gives the same value as from Eq. 6 since the concentration of C^*B is negligible. The conductance PS is here considered purely passive, involving no transporter.

Figure 4 shows the effect of adding tracer to the system after equilibration of tracee has occurred between the two chambers and between free and bound forms in V_1. The shape of the relaxation curve for C_1^* (t) in V_1 is different for increases in k_{ON} *(top panels)* compared to increases in *PS (bottom panels)*. Increasing *PS* from 0.1 ml/s to higher values leads to rapid entry of C into V_2, resulting in an overshoot in C_2 above the final equilibrium value. This overshoot has the effect of actually prolonging the transient, as can be seen by comparing the tails of the tracer curves (right panels) for *PS* = 0.1 ml/s and *PS* = 1.0 ml/s, the latter converging more slowly. The reason for this is that the early loss into V_2 causing the same overshoot for C_2^* as was seen in the first few seconds for the non-tracer C_2, this renders it unavailable to the binding site in V_1 after it returns from V_2 to V_1. Mechanistic modeling of this sort reveals phenomena that are not intuitively obvious. This would not be evident in straightforward compartmental modeling with constant coefficients.

Model 1.D: Instantaneous Versus Slow Tracer Binding in Tracee Steady State Situations

When binding is instantaneous the effective volume of distribution for tracer is determined solely by the steady state concentrations of tracee and binding ligand:

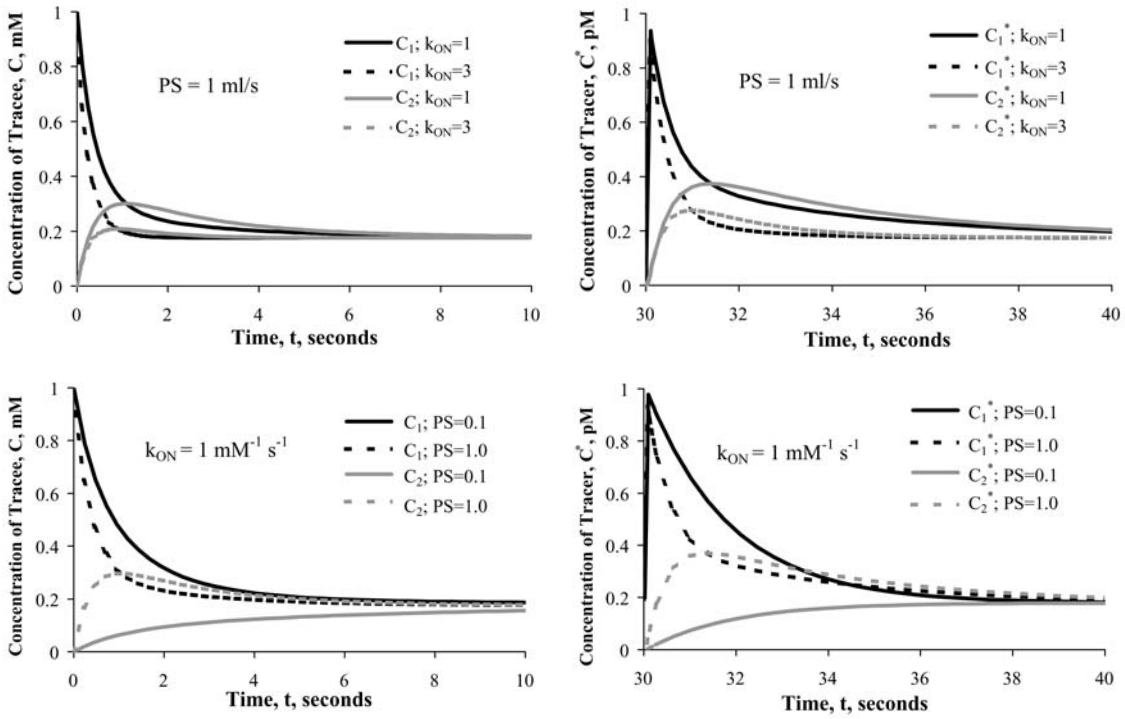

Figure 4: Tracer added (right panels) after tracee and binding site have equilibrated (left panels) with K_D=0.1 mM, B_T=1 mM, and V_1=V_2=1 mM. Curves denoting tracer transients in right panels follow equilibration in left panels. *Top panels:* With *PS* constant at 1 ml/s, increasing k_{ON} reduces the time for tracee (left panel) tracer (right panel) equilibration. *Bottom panels*: With k_{ON} = 1 $mM^{-1}s^{-1}$ (1% of that in Figure 3) and K_D is constant, increasing PS from 0.1 to 1.0 ml/s produces a faster initial part of the tracer transient (from 30 s < t< 35 s) but the actual time to equilibration is actually lengthened, having a long low tail. For both pertubations, the overshoot in C_2 is less than the overshoot in C_2^* because of non-linear kinetics resulting from binding site disequilibrium.

$$\frac{dC_1^*}{dt} = -\frac{PS}{V_1}\cdot\frac{(C_1^* - C_2^*)}{(1 + B_T/(K_D + C_1 + C^*_1))} = -\frac{PS(C_1^* - C_2^*)}{V_1^p} \qquad (20)$$

where C_1 in the denominator denotes the constant mother concentration. (Second order terms in the derivative are ignored.) Because C_1^* is orders of magnitude smaller than C_1 (the definition of a tracer), the denominator on the right side equals V_1^p as in Eq. 13. The tracer C_2^* equation is the same as Eq. 19. Equations are not needed for *CB* or *B* since the information is accounted for in the denominator of Eq. 20.

The coefficients in Eqs. 19 and Eq. 20 are only constant when the mother solute is in steady state. Then and only then, the tracer equations are linear, with constant coefficients. From this it seems obvious that the tracer transient equations could simply use the coefficients for the mother

substance; for example, if the *PS* for the membrane represented the conductance for a non-linear facilitating transporter, then using its value at the particular C_1 and C_2 for the mother substance in steady state would be exactly correct for the tracer in the transient. This is true for processes involving conductances but not for volumes of distribution, as will be seen by examining tracer transients for this system.

Examine the situation when k_{ON} is 10^4 $mM^{-1}s^{-1}$, resulting in effectively instantaneous equilibration between C_1 and *B*, as in the *top panel* of Figure 5. Starting from initial conditions C_1=C_2=0, a 1 mM pulse of C is introduced into compartment 1 and equilibrium is achieved in less than 5 seconds. At t = 10 seconds, a bolus of tracer is injected into V_1. The tracer concentrations, C_1^* and C_2^* were calculated in two ways, using equations describing slow binding, Eqs. 16 to Eq. 19, and then using equations describing instantaneous binding, Eqs. 19 and Eq. 20. The results show that the two methods give identical results (within about 0.0001 mM using the solver CVODE) and that Eq. 20 is correct when the binding rate is truly fast.

The *bottom panel* of Figure 5 illustrates the error caused by applying the instantaneous equilibrium assumption to a system with slow binding, k_{ON} = 1 $mM^{-1}s^{-1}$. Shown are the "true" tracer curves for the tracer concentrations, C_1^* (thick solid) and C_2^* (medium solid) and for C^*B (thin solid), using the slow binding model of Eqs. 16 to Eq. 19. The same three concentrations calculated from the instantaneous binding model of Eqs. 19 and Eq. 20 are shown as corresponding gray dashed lines. As expected, the two models predict quite different tracer profiles. The solid lines, which account for the slow binding kinetics, display transients that are quite different from the instantaneous binding model. C_1^* now has a high early peak, as does C_2^* but C^*B shows a slow monotonic rise to ist equilibrium level. The dashed curves are unchanged from the *upper panel* by the change in k_{ON}, of course, as the assumption for Eq. 20 is that equilibration is instantaneous.

Estimating model parameters while making the erroneous equilibrium assumption:

Analyzing observed tracer data using an equilibrium (i.e., fast) binding assumption is often correct as shown in the *top panel* of Figure 5 and might be considered reasonable if we hadn't been subjected to the slow binding situation presented in the *bottom panel*. Thus, it is interesting to determine what might be the parameters estimated by fitting the solid lines of the *bottom panel*, which are correct solutions, with the equilibrium-based model described by Eqs. 19 and Eq. 20. (To do this in JSim using an optimizer, one exports the text file of results in the *bottom panel* of Figure 5, then imports it as "data" into the same project file, allowing the curve of C^* "data", open circles, to be chosen and fitted with the model solutions based on Eqs. 19 and Eq. 20.)

The result shown in Figure 6, *top panel*, is that the 2-equation pseudo-equilibrium model can give a good fit of C_1^* to the "data", the correct solution shown by the thin continuous line, but at a cost. One cost is sacrificing accuracy in estimating the real kinetic parameters. The second cost, not so obvious if one only observes C_1^*, is the failure to predict C_2^* "data", closed circles, with the true 3-equation solution for C_2^* as indicated by the thick continuous line. The *bottom panel* shows how the parameters diverge from the correct values as they converge on a fit for C_1^*. The results of a set of seven optimization runs, Table 1, shows that the reduced model has little sensitivity to either B_T or K_D because their final values vary widely for very close fits of the "data". The estimates for *PS* are quite consistent, being about 25% higher than for the original "data ", and estimates of V_2 are consistently over twice the correct value, while estimates of V_1 are mostly low and widely scattered. However, the table reveals significant *covariance* amongst

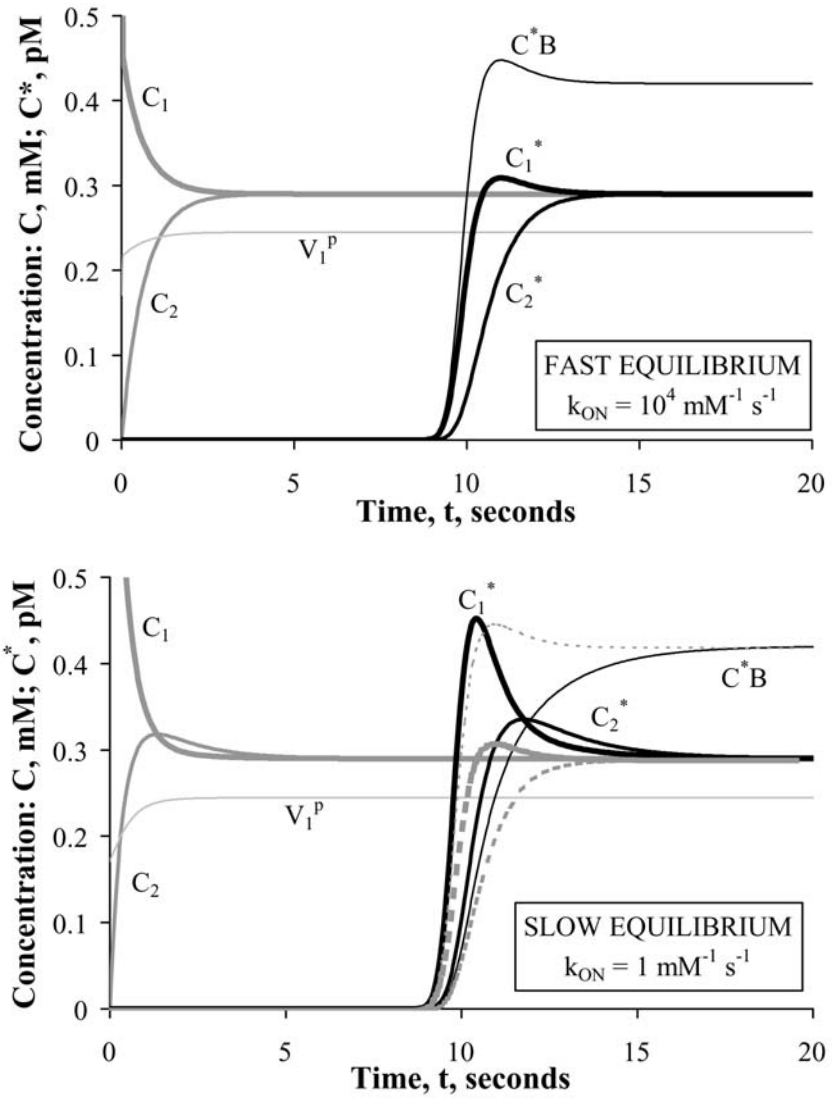

Figure 5: Tracer transients, C^* , when there is solute binding and permeation. Model parameters are B_T = 1 mM, K_D = 0.4 mM, $V_1 = V_2$ =1 ml, PS = 1 ml/s. At t = 10 s, a bolus of tracer is inserted into V_1 as a narrow Gaussian pulse (mean time = 10 s, standard deviation = 0.5 s). *Top panel*: Fast binding, $k_{ON} = 10^4$ mM^{-1} s^{-1}. Results are the same for C_1^* using either Eq. 16 or Eq. 20 for C_1^* . For this fast equilibration situation, Eq. 20 is correct. *Bottom panel*: Slow binding, k_{ON} = 1 mM^{-1} s^{-1}. Results for C_1^* and C_2^* from t=9 to t=15 seconds using Eqs. 16 to Eq. 19 differ dramatically from those using Eq. 20 for C_1^* , showing that Eq. 20 is erroneous even though the system for mother substance is in steady state. The linearization, using an equilibrium-based coefficient in Eq. 20, is inappropriate when a capacitance is involved and that capacitance is changing more slowly during the tracer transient than is assumed for the coefficient in Eq. 20.

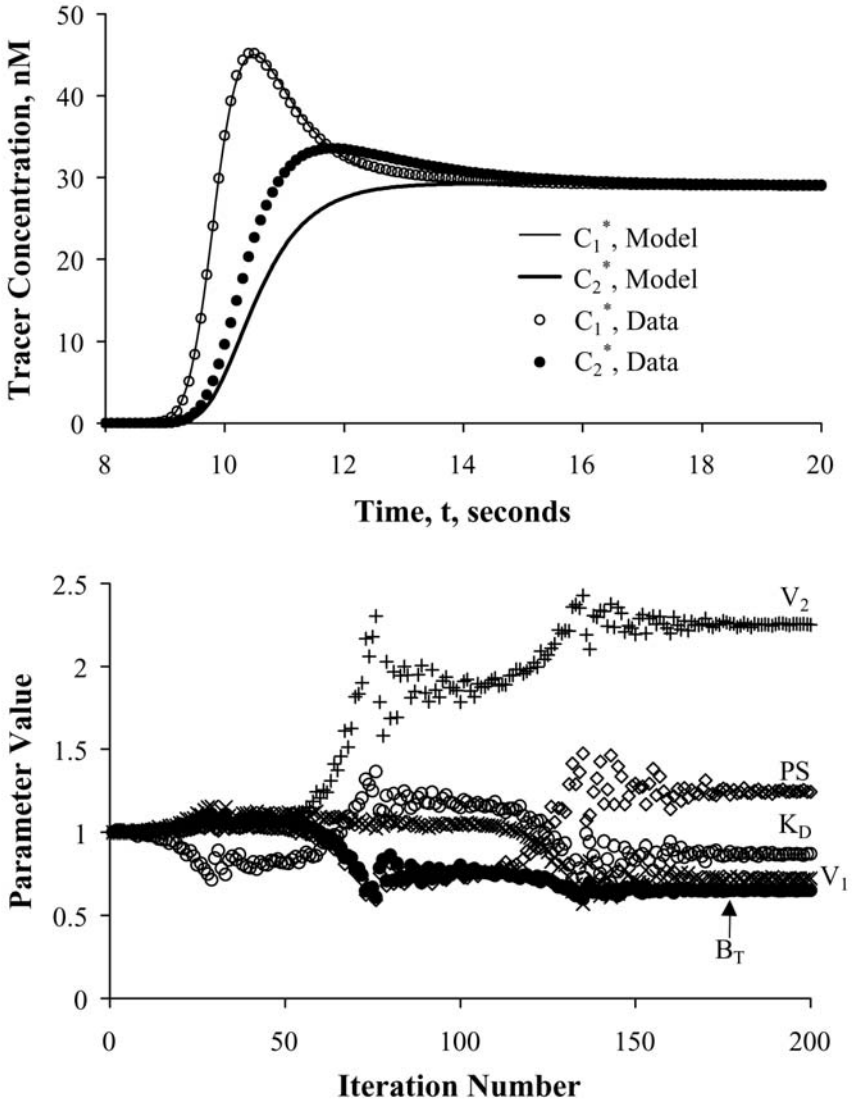

Figure 6: Optimization trial of the 2-equation pseudo-equilibrium model to fit C_1^* "data" on tracer transient computed using the full 3 equations. *Top panel*: The model curve (thin line) fits the "data" (open circles) for C_1^*, but the parameters are different. (The "data" curve from the true 3-equation model C_2^* (closed circles), not included in the objective function since it would normally not be observed, is well above the model solution for reduced 2-equation model C_2^* (thick line) during the transient, though the 2-equation model is close to the correct steady state level at t = 20 s. *Bottom panel*: The optimized parameters were started at the correct values (except for K_D) for the mother substance, and diverged to quite different values (Table 1, Trial 6) to achieve a good fit to C_1^* . See Table 1 for results of the other Trials.

Table 1: Results of Optimizing the 2-Eq Equilibrium Model Eq. 19 and Eq. 20 to Fit 3-Eq "Data" as shown in Figure 6.

Parameter	*Original Values*	Trial 1	Trial 2	Trial 3	Trial 4	Trial 5	Trial 6	Trial 7
B_T	1.0 mM	0.734	0.014	0.562	0.045	0.201	0.651	2.229
K_D	0.4 mM	0.813	0.033	0.008	0.252	0.001	0.869	0.485
PS	1.0 ml/s	1.247	1.246	1.247	1.246	1.246	1.246	1.246
V_1	1.0 ml	0.671	1.116	0.038	1.073	0.483	0.723	0.230
V_2	1.0 ml	2.254	2.254	2.254	2.254	2.254	2.254	2.254
RMS error		221.9	221.9	220.5	221.9	221.8	221.9	221.9

parameters, e.g. the low estimates of V_1 are associated with high affinity of the binding site (low values of K_D). This is to be expected since B_T was kept at 1 mM and not allowed to adjust in the optimization. Since it is mass or quantity that counts, when the affinity chanced to increase in the optimization, the volume of compartment 1 decreased. To compensate, compartment 2 volume increased in order to fit the downslope of the model curve after its peak and to keep the time constant of the transient of the order of V_2/PS .

Supposing that the only observable variable is C_1^* , how then could one avoid an errorneous interpretation of the configuation of the system? Since C_1^* can be fitted nicely with a 2-compartment model, how would one know that 1) there is a binding site; and 2) the system compartmental volumes and the PS are wrongly estimated? The first part of the answer is to use other information. Are the estimates of V_1 and V_2 in accord with the known anatomy? That comparison gives a good clue if other data on V_1 and V_2 are available. The second part of the answer is that the concentration of mother substance should be measured. Then the concentration of mother substance should be raised and the experiment repeated. The K_D is presumably unknown, but if the concentration happened to be raised from below to above the K_D, the binding site will be revealed. If the original C_1 was far below the K_D, a decade increase in C_1 may not suffice to change V_1^p but if the original C_1 was greater than about $0.01K_D$ then a diminution in V_1^p at the raised concentration will reveal the presence of B, allow a crude estimate of B_T and K_D, and certainly provoke doing further experiments to estimate them accurately.

Another approach is to ignore the possibility of binding being involved in the form of the data curves, To do this one sets the value of B_T to zero, removes both k_{ON} or K_D from the parameters to be optimized, and proceeds to obtain a best fit of the same 2-Eq model to the 3-Eq model solution. The results in Figure 7 demonstrate that the fit is just as good as with the more complete model, with the root mean square error being 221.9, comparable to those in Table 1, but the parameters differ: V_1 is 1.159 ml, V_2 is 2.25 ml, and PS is almost unchanged at 1.245 ml/s. As before, change in apparent volumes make up for the accumulation of bound ligand in the original system. The lesson here is that an incorrect model is not necessarily going to be invalidated by comparison with a parsimonious data set that includes no information on the actual volumes in the real system. If anatomic data had defined these volume to within 10 or 20% of correct values then the analyst would have noted the disparity between estimated and real volumes, particularly for V_2, and would have been more likely to incorporate the binding site into the model.

The summed volumes for the three parameter fit have to account for the total mass of tracer injected, even though B_T was set to zero and the final part of the curve for C_1^* had to match that

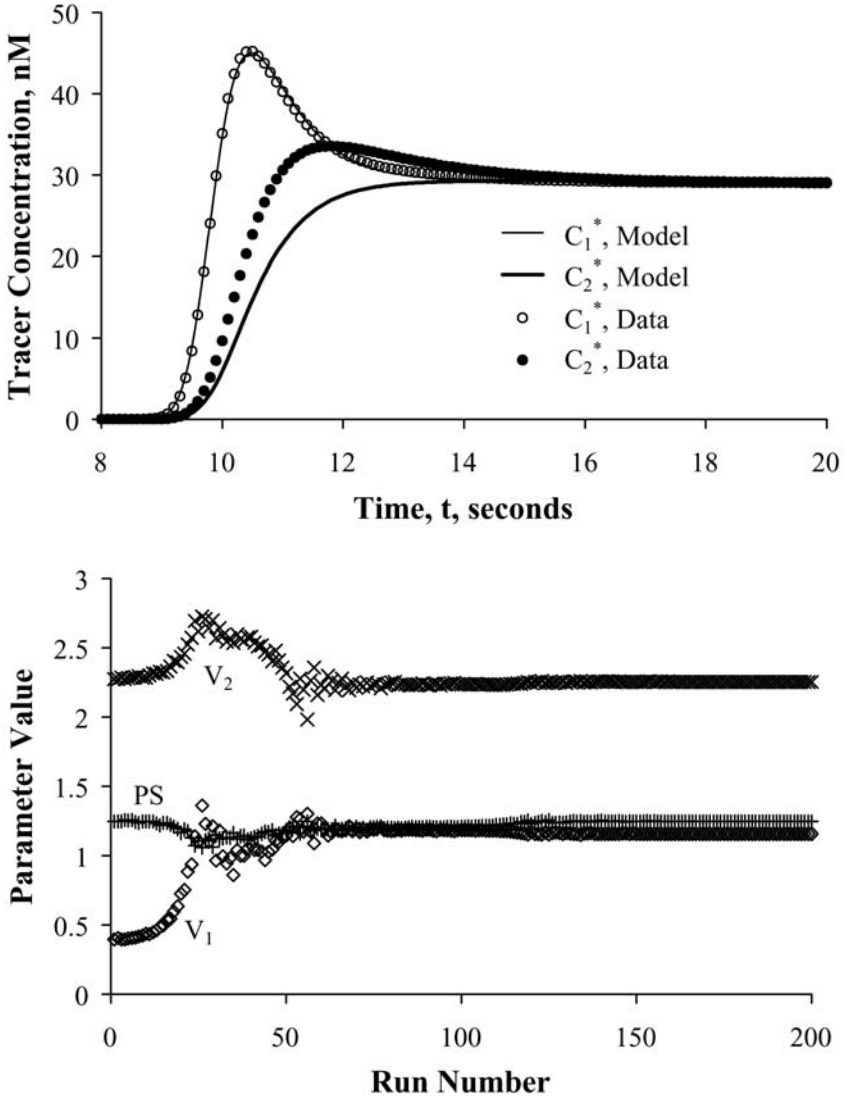

Figure 7: Optimization to fit the 2-Eq model to the 3-Eq model solution assuming the absence of any ligand binding in V_1 or V_2. The matching of the C_1^* data (open circles) by the 2-Eq model is as good as that in Fig 6, but the parameter values are different; the error in C_2^* is about 25% when t=12s. Estimated values: V_1 = 1.159 ml, V_2 = 2.254 ml, and PS =1.246 ml/s. Correct values: V_1 =1 ml, V_2 =1 ml, PS =1 ml/s, B_T =1 mM, and K_D = 0.4 mM.

from the data where binding was included. Therefore the sum of the tracer mass in Figure 5 has to match the sum in Figure 7, i.e. $V_1C_1^* + V_2C_2^* + V_1C^*B$ in Fig 5 = $V_1C_1^* + V_2C_2^*$ in Fig 7 , which is exactly so. In Figure 5 the final values of C_1^* and C_2^* were both 0.29 x 10^5 pM and C_1^*B was 0.42 x 10^5 pM for a total of 10^5 pmole. In Figure 7 the total estimated volume is 3.41 ml and the final concentration is 0.293 x 10^5 pM giving a total of 10^5 pmole injected and retained in the system.

Mass is conserved! Cobelli et al (2000, Chapter 7) make this point nicely, and further argue that using anatomic information narrows the confidence limits for parameter estimates.

The first lesson from Figure 7 is that the data can be fitted without any consideration of either binding or of anatomical constraints, but that ALL of the parameter estimates were erroneous. Though the virtual volume of distribution was correct, the total anatomic water volume was overestimated by 70% and the *PS* by 25%. Thus linear compartmental analysis was misleading. If the K_D had been 0.1 mM, as in Figure 2 instead of 0.4 mM, then the errors would have been larger, as the total volume of distribution would have been 12 instead of 3.4 ml. This difference would have been observed if the tracer had been injected at two different known levels of mother substance.

The second lesson from Figure 7 is that it is important to measure the background, native solute concentration when doing tracer experiments in order to interpret the results in terms of the underlying physiology and biophysics. For example, when another solute is added to the system, the rate coefficient PS/V_1^p in Eqs. 19 and Eq. 20 might be changed. Additionally, it may be useful to consider how one might detect or identify changes in the following: (a) *PS* (e.g. changing width of a channel); (b) the level of free binding sites, *B* (e.g. reduced by B binding to the new solute); (c) K_D (e.g. by an allosteric effect on the binding protein); (d) C_1 (e.g. by influencing some other reaction involving C in either V_1 or V_2); or (e) V_2 (e.g. by shrinking or expanding the cell volume). While this list is hardly exhaustive, the idea is to contemplate the effects of other possible influences, as a routine check.

II. CAPILLARY-TISSUE EXCHANGE: CONVECTION, PERMEATION, REACTION AND DIFFUSION

The two-compartment system from Figure 1 is here modified to incorporate flow, as shown in Figure 8, thus identifying V_1 as the vascular region, the membrane as the capillary barrier, and V_2 as the tissue. The system is considered as a homogeneously perfused organ with constant volumes and steady flow *F* in and out. Now, in order to put it into the context of substrate delivery and metabolism, we switch to standard physiological representation of the units, defining them per gram of organ mass. *F, PS,* and the consumption *G* have units ml $g^{-1}min^{-1}$, and the volumes have units ml/g. This notation normalizes flows, substrate use, etc. to be independent of organ mass.

To keep the system simple so as to focus on the blood-tissue exchange, the intratissue consumption is considered to be a first order process, as if the substrate concentration is far below the K_D for an enzymatic reaction. The PS however is treated as a facilitated transport process reduced in form to symmetric Michaelis-Menten type kinetics. (There are several assumptions necessary for this simplification: instantaneous equilibration of substrate to transporter binding site at both surfaces, bidirectionally identical rates at same rates for free and substrate-bound transporter, no effect of transmembrane charge, rates independent of concentrations of other solutes, reaction product not transported by the same carrier.)

A technique developed to distinguish individual processes involved in blood-tissue exchange and reaction was the **Multiple-Indicator Dilution (MID) technique**. It was used first by Chinard (1953, 1955) for the purpose of estimating the volumes of distribution for sets of tracers of differing characteristics: the mean transit time volume, $V_{mtt} = F \times t$, where t is the mean transit time through the system. He did not estimate permeabilities as his studies were on highly permeable solutes. Crone (1963) analyzed the technique, showing how it could be used to

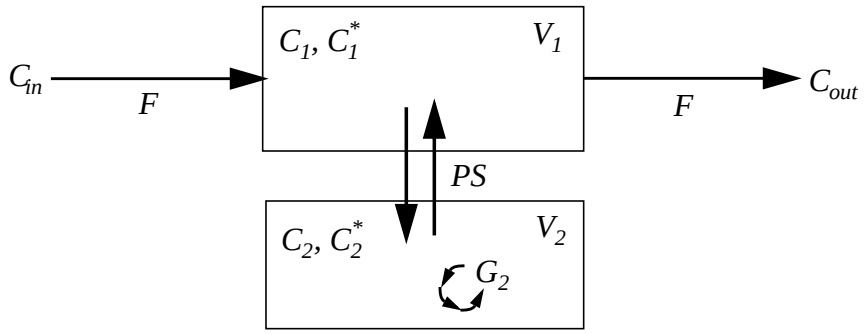

Figure 8: A two compartment system for the facilitated exchange of solute C between flowing blood and surrounding stagnant tissue. Solute binding in the blood is neglected in this example. Flow F, $g^{-1}min^{-1}$, carries in solute at concentration C_{in}, mM, and carries out a concentration C_{out}, mM. The rates of permeation or reaction for tracer C^* are determined by the concentration C of tracee or mother solute. PS, ml $g^{-1}min^{-1}$, is a conductance, the permeability-surface area product of the membrane separating the two chambers, allowing bidirectional flux. G_2 ml $g^{-1}min^{-1}$, is a reaction rate for a transformation flux such that the product G_2 C_2 is mmole $g^{-1}min^{-1}$,.

estimate *PS* from the outflow curves for a simultaneous injection into the inflow of a solute and impermeable tracer as shown in Figure 9, which diagrams an experimental setup for examining the uptake of D-glucose in an isolated perfused heart as by Kuikka et al. (1986). L-glucose, the stereo-isomer, serves as an extracellular, non-metabolized reference. A more realistic diagram of a capillary–tissue exchange includes the endothelial cells and interstitial fluid, ISF, as shown in Fig. 10.

To reduce this diagram to that of Figure 8 requires a further set of assumptions. For current purposes these are that the endothelial layer, the interstitial fluid space and the plasmalemma of the parenchymal cell can be represented by a single membrane, within which resides the transporter with conductance PS This ignores the capacitance of these structures, which include receptors and transporters.

To determine capillary permeability the relevant reference solute is one that does not escape from the capillary blood during single transcapillary passage; for example, albumin is the relevant reference solute to determine the capillary permeability to glucose. In this situation the albumin dispersion along the vascular space may be assumed to be the same as that of the glucose; thus the shape of the albumin impulse response, $h_{alb}(t)$, accounts for the intravascular transport of all the solutes. (L-glucose, an extracellular reference tracer with the same molecular weight and diffusivity as D-glucose, is the extracellular reference for D-glucose, having the same capillary PS_c and the same interstitial volume of distribution, V_{isf}. Having simultaneous data on such reference tracers greatly reduces the degrees of freedom in estimating the parameters of interest for D-glucose,)

While we have fully developed mathematical models for the system diagrammed in Fig. 10 (for example, Bassingthwaighte, Wang and Chan, 1989 and Bassingthwaighte Chan and Wang, 1992), including ones with facilitating transporters and sequences of reactions (Bassingthwaighte

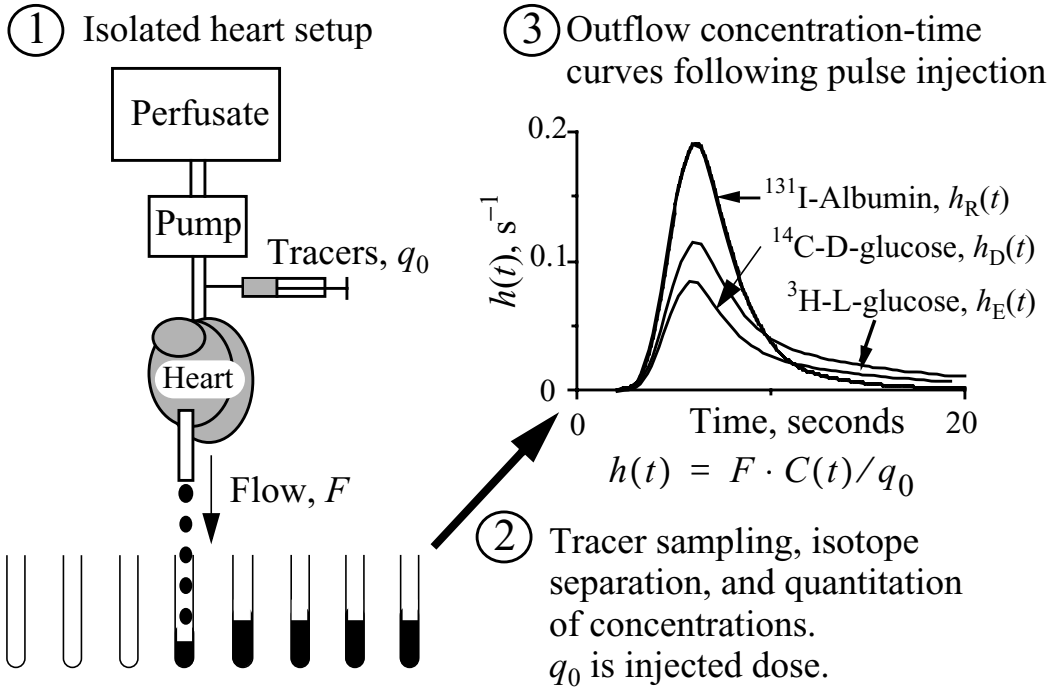

Figure 9: Schematic overview of experimental procedures underlying the application of the multiple-indicator dilution technique to the investigation of multiple substrates passing through an isolated organ without recirculation of tracer. The approach naturally extends also to their metabolites.

et al., 2006), our present purpose is assess the accuracy of estimates of the permeability, PS, of the capillary barrier to a solute.

An ideal set of reference solutes for evaluating a Fig. 10 model is listed in Table 2. Fitting MID concentration-time curves for the first three classes of solutes with the model solutions provides estimates of the parameters listed in the right column, and approximates or even gives exactly the parameter values for the test substrate. For the test substrate the observed data are fitted using only the few remaining free parameters for binding and reaction. To examine the effects of model reduction, we will use only the intravascular reference marker and the solute of interest which enters the parenchymal cell, of which V_2 in Figure 8 is the analog.

Model Equations for Tracer:

The diagram in Fig. 10 differs dramatically from that of Figure 8, but with the assumptions listed above reduces to the same model. Even so, one might debate what type of equations to use. Capillaries are of the order of 1 mm long, and are 5 microns in diameter, an aspect ratio of 200 times. Consequently, considering the capillary as a stirred tank is impossible. Diffusional relaxation times differ by a factor of 200 between radial and axial directions. The stirred tank expressions, with no intravascular binding, are the same as Model 1B except for the addition of the flow through compartment 1 and the consumption term G_2 to the second compartment, and the omission of binding from the first:

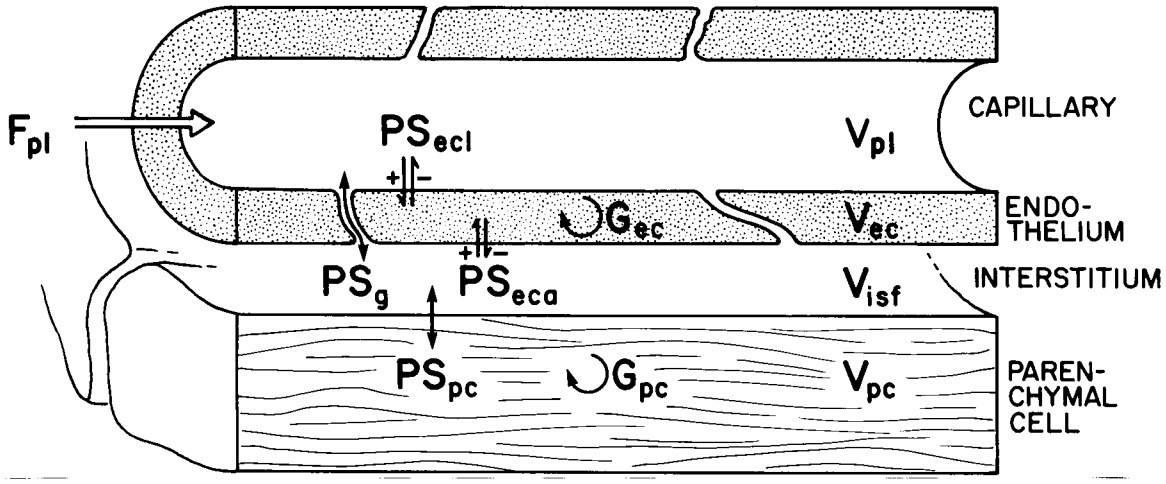

Figure 10: Representation of a blood-tissue model used for analysis of indicator-dilution curves. *F*, plasma (perfusate) flow, ml g^{-1} min^{-1}, PS, permeability-surface areas, ml g^{-1} min^{-1}, for passage through endothelial cell luminal membrane (PS_{ecl}); water-filled channels or gaps between endothelial cells (PS_g); endothelial cell albuminal membrane (PS_{eca}); and parenchymal cell membrane (PS_{pc}). *G*, intracellular consumption ml g^{-1} min^{-1} (metabolism) of solute by endothelial cells (G_{ec}) or by parenchymal cells (G_{pc}). *V*, ml g^{-1}, volume of plasma (V_{plasma}), endothelial cell (V_{pc}), interstitial (V_{isf}) and parenchymal cell (V_{pc}) spaces, the anatomic volumes, ml/g. (Figure from Gorman et al., 1986, with permission from the American Physiological Society.)

Table 2: Reference tracers for a substrate

Solute class	Example	Information provided by the solute class
Intravascular	Albumin	Convective delay and dispersion in all vessels perfused
Extracellular	L-glucose	Cleft PS_g, and interstitial volume, V'_{isf}
Unreacted but transported analog	3-O-methyl -D-glucose	Cell PS_{pc}; intracellular volumes of distribution, V'_{pc} and V'_{ec}
The test substrate	D-glucose	Binding space; reaction rates inside cells, G_{ec}, G_{pc}

$$\frac{dC_1^*}{dt} = \frac{F}{V_1}(C_{in} + C_{out}) - \frac{PS}{V_1} \cdot (C_1^* - C_2^*) \quad \text{, and} \tag{21}$$

$$\frac{dC_2^*}{dt} = \frac{PS}{V_2}(C_1^* - C_2^*) - \frac{G_2}{V_2} \cdot C_2^* \tag{22}$$

The use of these ordinary differential equations (ODEs) implies and assumes a discontinuity between the concentration of solute in the inflow and that in V_1. Because V_1 is assumed instantly mixed the tracer entering the tank is immediately available to be washed out with the same probability as any molecule dwelling in there for a longer time. In view of the long capillary length and slowness of diffusion, the mixing chamber idea is untenable, unless there is no gradient in solute concentration along the capillary.

The capillary-tissue unit of Fig 10 can also be reduced to two regions represented by partial differential equations (PDEs) that allow continuity along the path between entrance and exit. Using the spatially distributed analogs for plasma, C_p, or blood, and extravascular tissue, C_{tiss}, to represent the lumped variables C_1 and C_2:

$$\frac{\partial C_p(x,t)}{\partial t} = \frac{-F_p L}{V_p} \cdot \frac{\partial C_p}{\partial x} - \frac{PS_c}{V_p}(C_p - C_{tiss}) + D_p \frac{\partial^2 C_p}{\partial x^2}, \tag{23}$$

$$\text{and } \frac{\partial C_{tiss}(x,t)}{\partial t} = \frac{-PS_c}{V'_{tiss}}(C_{tiss} - C_p) - \frac{G_{tiss}}{V'_{tiss}} C_{tiss} + D_{tiss} \frac{\partial^2 C_{tiss}}{\partial x^2}. \tag{24}$$

where C_p and C_{tiss} are spatially distributed functions of both x and t, not just t. The axial position is denoted by x, where $0 < x < L$, the capillary length, cm. In the modeling the analogy is $F_p = F$, $V_p = V_1$, $V_{tiss} = V_2$, and $PS_c = PS$, the permeability-surface area of the capillary wall, but we retain the two sets of names in order to make comparisons between the estimated parameter values. The capillary length is arbitrarily set to an average value such as 0.1 cm. PDEs require boundary conditions: at the capillary entrance, $C_p(x=0, t) = C_{in}$, so there is no discontinuity in the concentration profile; at the exit $C_{out} = C_p(x=L, t)$, as a result of the no-flux boundary condition and the same condition described by the ODEs. The last term in each equation is the diffusion along the length of the capillary-tissue regions; the use of an anatomically correct length then makes using observed diffusion coefficients for D_p and D_{tiss}, cm^2/s, practical and meaningful. Gross exaggeration of the diffusion coefficients can be used in the equations to turn the distributed model into a *de facto* well-mixed, compartmental model.

The flow term merits further explanation since it might appear that the sign in the first right-hand side term of Eq. 23 differs from that of Eq. 21. Consider the inflow to contain a bolus of solute: as it enters, the concentration at the capillary entrance rises. At this time, the slope of the curve of concentration versus position x, $\partial C/\partial x$, is negative; the spatial slope has always the sign opposite to the temporal derivative $\partial C/\partial t$ at the same point, thus the negative sign on the term.

Functionally, therefore Eqs. 23 and Eq. 24 are analogous to Eqs. 21 and Eqs. 22. But using the PDEs avoid the unrealistic discontinuity in the compartmental model at the entrance, which is the corollary to the instantaneous mixing within V_1. Most important, the PDE allows continuity in concentrations and concentration gradients along the capillary, and not only in concentration but

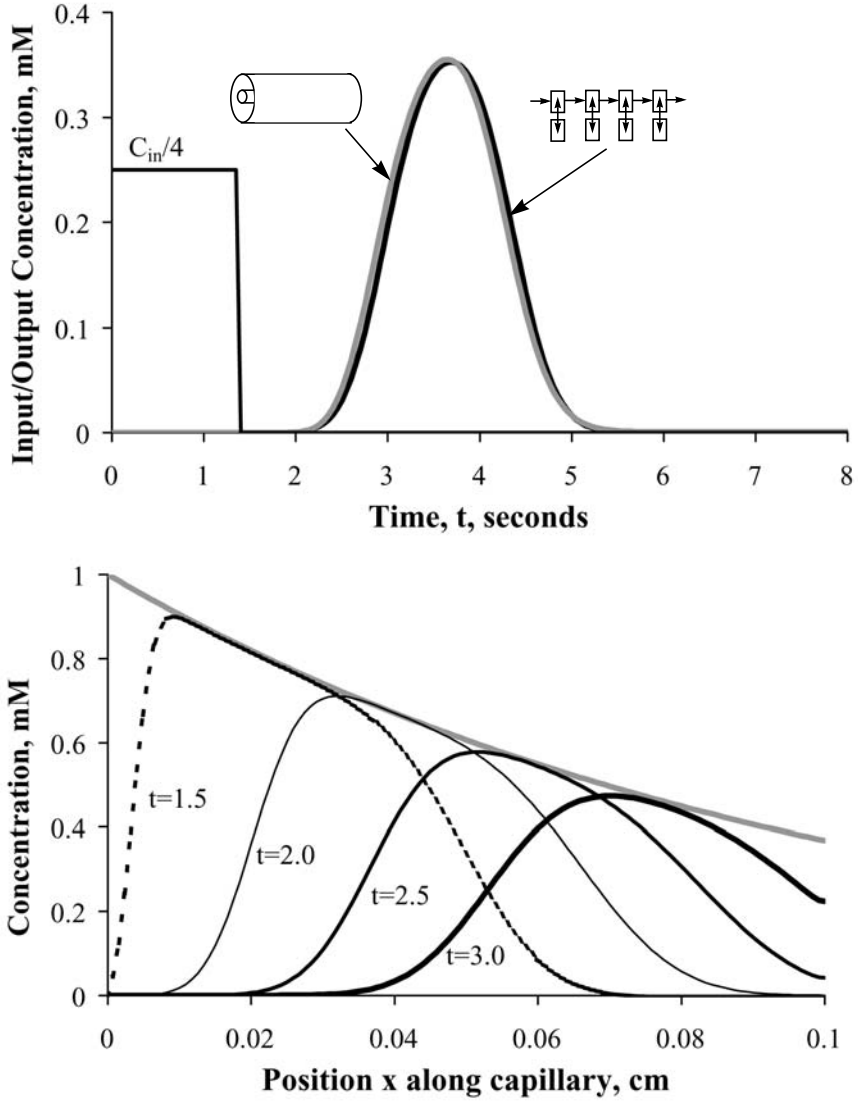

Figure 11: Pulse responses in axially-distributed models. The input function, C_{in}, is a pulse of duration 1.4 seconds. *Top panel*: Outflow concentration-time curves for (gray curve) a PDE numerical solution using a Lagrangian sliding fluid element method and an intravascular dispersion coefficient, Dp = 2.6 x10^{-5} cm^2/s, and for a serial stirred tank algorithm representing a Poisson process with 109 stirred tanks (black curve almost superimposed on the gray one). *Bottom panel*: Intracapillary spatial profiles at a succession of times, 1.5, 2.0, 2.5, and 3.0 seconds, as the pulse disperses and some of the solute permeates the capillary wall. Parameters were the same for the Poisson model and the PDE: F_p = 1 ml g^{-1} min^{-1}, PS_C = 2 ml g^{-1} min^{-1}, and tissue volume V_{tiss} was set to 10 ml g^{-1} so that there was no tracer flux from tissue back to the plasma space.

also in the properties of the system such as axial gradients in transporter and enzyme densities that are evident in the liver sinusoid. For the following analysis, all parameters are assumed spatially uniform so as to minimize the difference from the compartmental models. There are many ways of representing axially distributed convecting systems, and two are shown in Figure 11: the usual approaches solve the PDE using one of several PDE solvers (Poulain et al 1997 #10457), and here we used a Lagrangian method (Bassingthwaighte et al 1992 #10371). A compartmental type of alternative is to approximate the capillary as a series of stirred tanks, each with the same volume and PS. With a large number of serial stirred tanks the longitudinal concentration gradient is approximated well as the steps from one to the next are small. The intravascular transport process with serial stirred tanks is a Poisson process. In modeling, serial stirred tanks are convient because the number of tanks can be used as a free parameter: the relative dispersion over the length of the tube is determined by N_{tanks} such that the relative dispersion RD, which equals the coefficient of variation, induced during transit is $1/\sqrt{N_{\text{tanks}}}$, so that with 100 tanks the RD is 10%.

Figure 11, top panel, shows curves for the PDE solution and for the Poisson process that are essentially similar, so that the dispersion coefficient D_p sufficed to create the same dispersion as occurred with the Poisson process using 109 tanks. The permeative loss is the same for both methods, with the result that the peak outflow concentrations are similar. Figure 11, bottom panel, shows the shape of the bolus as a function of position as it deforms ever more from its initial square pulse at the entrance to the capillary. Because the capillary PS > 0 there is loss of solute as the bolus progresses along the capillary: the diminution in peak height is therefore due not only to the spreading but to the loss. This loss is reflected of course in the reduction in the areas under the successive plots of $C_p(t, x)$ as solute escape into the extravascular region. (For this illustration the value of V'_{isf} is set so abnormally high that C_{isf} remains negligible and there is no back flux from ISF to plasma.).

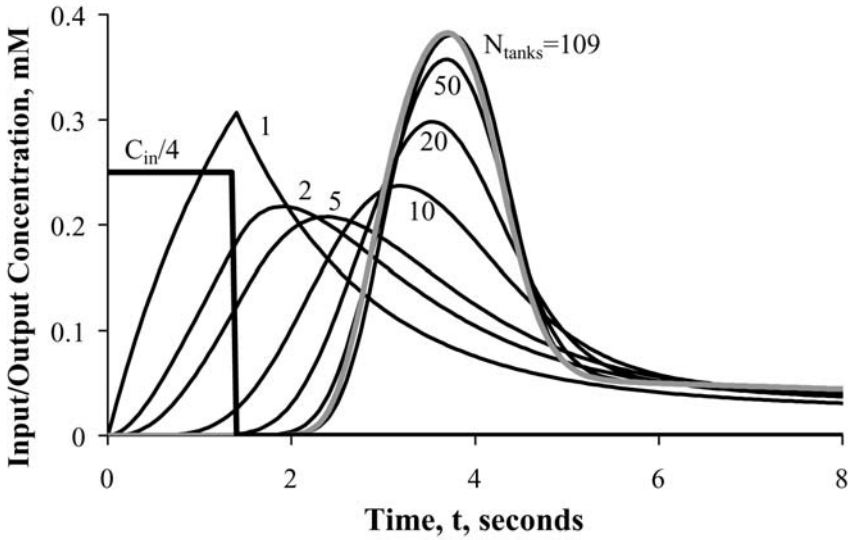

Figure 12: Responses of the Nth order Poisson operator with N_{tanks} varied from 109 tanks in series down to 50, 20, 10, 5, 2, and finally to a single mixing chamber, $N_{\text{tanks}} = 1$. The gray curve is the Lagrangian solution to the PDEs as in Figure 11. All of the Poisson operator (black) outflow curves have the same mean transit time, but differ in their shapes. The parameters were $V_p = 0.05$ and $V_{\text{tiss}} = 0.15$ ml/g; $F_p = 1$ ml g^{-1} min^{-1}, $PS_C = 1$ ml g^{-1} min^{-1},

While the Poisson operator with N_{tanks} set to a large number can be used to fit data, it is computationally less efficient than solving the PDE directly, and the additional disadvantage that the dispersion cannot be controlled independently of choosing N_{tanks}.The relative dispersion with N_{tanks} = 10 is 0.318, and with N_{tanks} = 1 is 1.0. While finite element grids for solving the PDEs can be rather coarse, e.g. 10 to 20 grid segments, in contrast when using the serial compartments N_{tanks} must remain high to get shapes anything like those of the experimentally observed curves. Figure 12 illustrates the dramatic shape changes brought about by reduction of N_{tanks} All of the Poisson operator outputs in the figure have mean transit times identical to that of the red reference curve. The solutions using low N_{tanks} have excessively long low tails to balance the too early peaks.

Fitting data with the model functions. We chose as an example a set of indicator dilution curves to which fitting a 3-region model is required, namely the uptake of adenosine in the heart wherein the endothelial cell metabolism is neglected and the capillary wall is considered as one membrane to cross, and thereby ignoring endothelial capacitance and reactions. The three regions are capillary plasma, ISF, and parenchymal cell, using the terminology of Figure 10, and the equations are Eqs. 23 and 24, the latter being for the ISF, and then adding a similar equation for the parenchymal cell and accounting for exchanges between ISF and parenchymal cell. (The 3-region model and the Lagrangian sliding fluid element method of solution are detailed in Bassingthwaighte et al. 1992). In Figure 13 are shown model fits to the three simultaneously

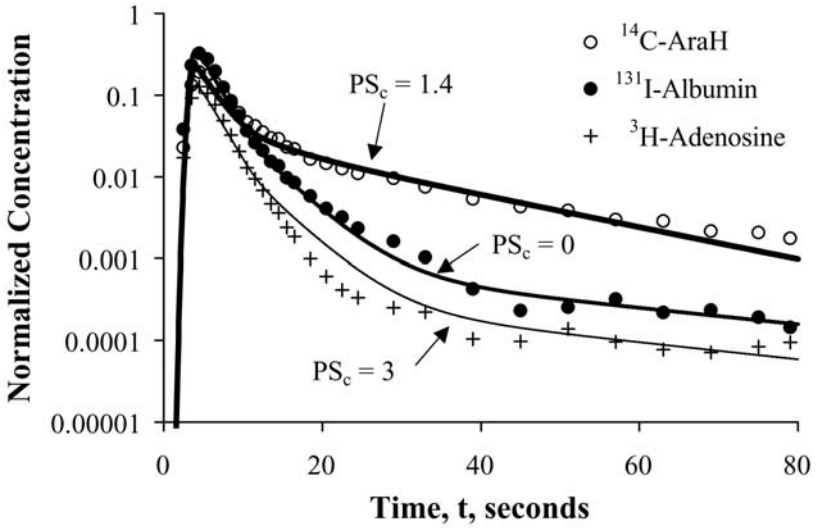

Figure 13: Multiple indicator dilution experimental curves fitted simultaneously with three-region PDE (shown) and serial compartmental models, using N_{tanks}= 80 for the latter (not shown but identical to PDE solution for long times). The parameters were V_p = 0.1 and V_{isf} = 0.4 ml/g; F_p = 2.8 ml g^{-1} min^{-1} (experimental value); PS_C = 0.019 ml g^{-1} min^{-1},for albumin, 1.3 for AraH, and 3.0 for adenosine; PS_{pc} = 25 ml g^{-1} min^{-1} and G_{pc} = 10^4 ml g^{-1} min^{-1} for adenosine (both zero for other tracers) and V_{pc} = 0.55 ml/g. Data from Schwartz et al. (2000).

obtained experimental curves. The Lagrangian PDE solutions for the three cases are essentially

identical to the serial stirred tank model solutions, using identical values for all of the physiological parameters, the flows, volumes, permeabilities, and consumption in the parenchymal cell, G_{pc}. The value for G_{pc} was set to a high value for this illustration and was not optimized, in accord with the fact that almost no tracer adenosine returns from the cell to the effluent plasma. The point of the Figure 13 is that so long as the models account appropriately for the intracapillary concentration gradients, the three anatomic volumes, the observed flow, and have the same intravascular dispersion, then the estimates of permeabilities are the same from the two models. When volumes and flows are the same then, by mass conservation, the mean transit times are forced to be the same.

However if the representation of the convective region is compromised by using fewer compartments, errors must be introduced into other parameters in order to fit the data. Figure 14 shows that the model solution can be obtained to fit the albumin data even with N_{tanks} as low as 15. Achieving such a result with N_{tanks}= 15 is fore-ordained with the method used here and has no scientific value; because are no data on the input function, an input function was constructed of arbitrary form by an iterative procedure (in effect a deconvolution) until the output at the known flow fitted the albumin curve, so the satisfactory fit is merely a self-fulfilling prophecy. If one wishes to fit the data with N_{tanks}< 15, then a new input function must be estimated so as to fit the albumin curve. This works for any number of tanks, illustrating that the choice of a model to fit the data is completely arbitrary and has no relation to the reality of the choice of a compartmental model. The corollary is that the anatomic and physiological parameters will be estimated erroneously. (*The lesson*: record the real input function during the experiment.).

Since it is often difficult experimentally to record the input function, this is a common predicament. What is demanded however, is that in order to elicit parametric information at the capillary-tissue exchange level one must use the *same* input function for the whole set of data curves, e.g. the set in Figure 13. The failure of compartmental analysis is exemplified by the results shown in Figure 15 with the same data set as in Figure 13. In the top panel, using N_{tanks}= 15 the parameters are almost the same as estimated using the PDE solution (Figure 13) or using N_{tanks}= 109. However, with N_{tanks}= 1 (bottom panel) the parameters are systematically different., overestimating PS_C at 20 compared to 3 and underestimating PS_{pc} at 7, compared to 20 ml g^{-1} min^{-1},while G_{pc} is only modestly underestimated at 60 compared to 90 ml g^{-1} min^{-1}. The interstitial volume, V_{isf}, is also underestimated at 0.20 ml/g compared to 0.33 to 0.4 ml/g. While for N_{tanks}= 1 (bottom panel) the input function allowed a good fit to the first 20 seconds of the curves, the tails could not be closely fitted. The single tank convective region forces the tail to become monoexponential. earlier than is seen for the more spatially distributed models. (They all become monoexponential eventually.) Table 3 shows the results for other values of N_{tanks}, where it can be seen that the estimates tend to deviate in a systematic fashion as N_{tanks} diminishes. As N_{tanks} diminishes from 15 to 5, 2, and 1, the estimate of PS_C rises 6 fold, PS_{pc} diminishes 30% for AraH and 70% for Ado, V_{isf} for AraH by 35%, V_{pc} rises 40% for AraH, and G_{pc} for Ado falls 30%.

The inference is clear. Given that one has trust in the physically realistic PDE version of the physical situation, constrained as it is by using values for the regional volumes taken from the anatomy, then the compartmental models systematically and progressively deviate from the physiological values even though the curves can be fitted not too badly. In no case did single stirred tank models fit well (N_{tanks}= 1, lower panel of Figure 15), but for larger values of N_{tanks} the fits were quite good. Now it is obvious that getting a good fit to the selected tracer dilution curves alone fails to guarantee sensible results. In every study there are other data, usually ignored, such

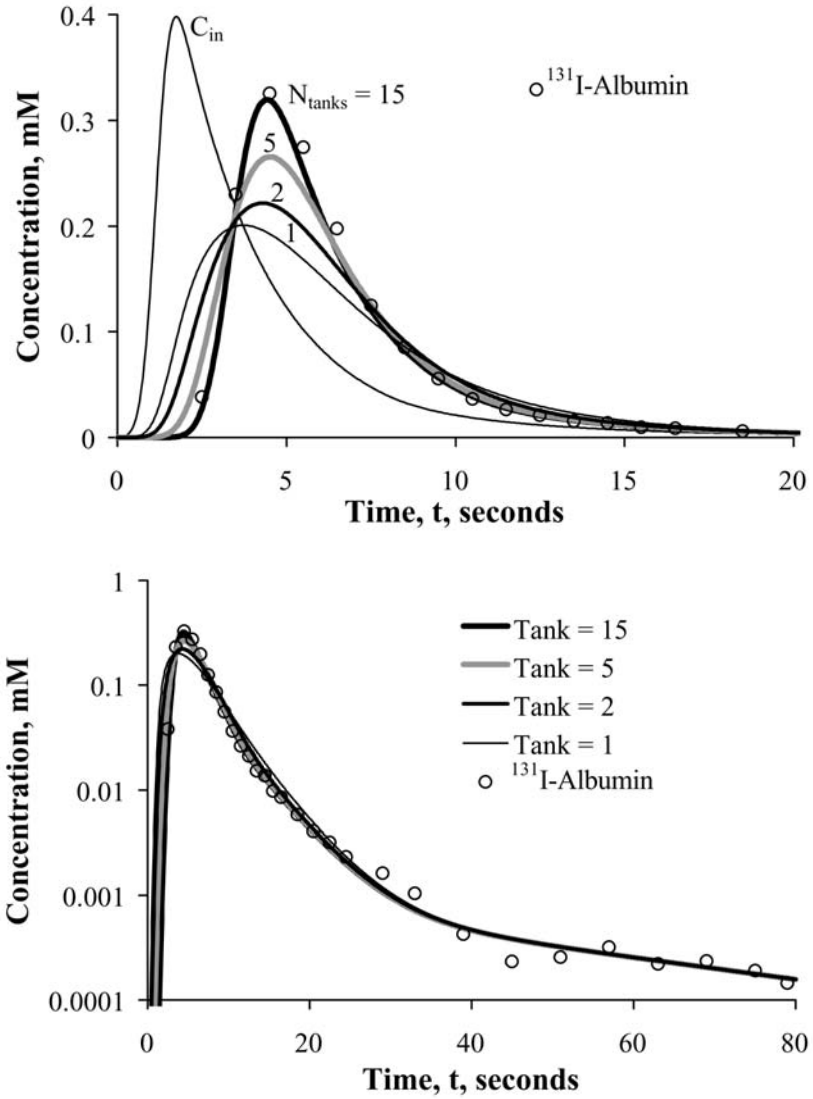

Figure 14: Fitting the intravascular reference ^{131}I-Albumin curve with the serial stirred tank model with N_{tanks}= 15 gives a good fit. *Top panel*: **Linear plot** showing short time transients. Using fewer compartments N_{tanks}= 5, 2, and 1, results in outflow concentration time curves that do not fit the experimental data, the model curves being too low peaked and too dispersed in time. *Bottom panel*: **Semilogarithmic plot** to show the whole data set. The misfitting of the upslope and peak of the curve which is so obvious in the top panel is less apparent (though it is exactly the same) but the tail of the albumin curve is fitted well by all of the models.

as the anatomy, other known physiological features, ionic or transmembrane charges, pH, previously identified reactions, binding sites and so on, that should be used in the analysis. When these “knowns” are incorporated into the scheme, and the basic conservation rules applied, then one starts to get physiologically valuable parameters *and* an understanding of the system.

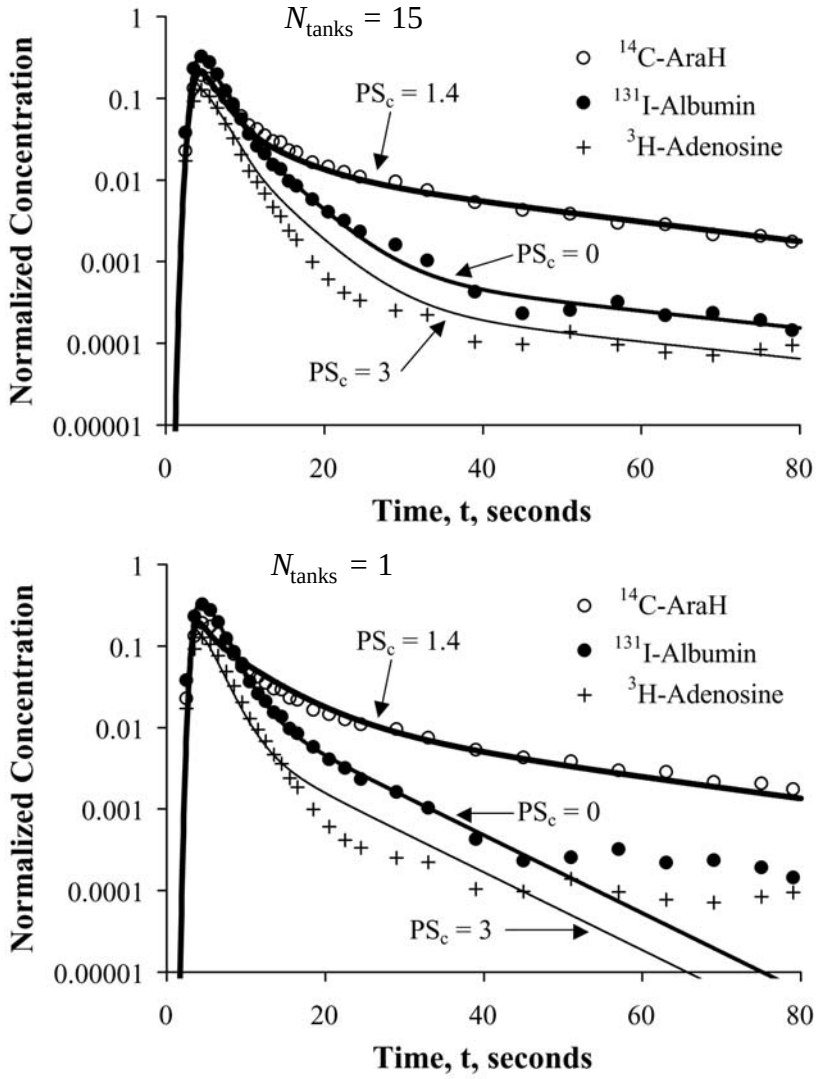

Figure 15: MID curves for ^{131}I-Albumin, ^{14}C-AraH, and ^{3}H-Adenosine fitted using the serial tank model and a common input function. *Top panel*: N_{tanks}= 15 as in Fig 14. Curves fitted almost as well as with the PDEs used in Figure 13. Parameters for the adenosine curve were F_p = 2.8 (experimental data), PS_C = 3, PS_{pc} = 20, and G_{pc} = 90 ml g^{-1} min^{-1}, with V_p = 0.11, V_{isf} = 0.33 and V_{pc} = 0.55 ml/g. *Bottom panel*: N_{tanks}= 1. The albumin curve is well fitted, but the input function differs from that used in the top panel. Parameters for the adenosine curve were PS_C = 3, PS_{pc} = 7, and G_{pc} = 60 ml g^{-1} min^{-1}, with V_p = 0.10, V_{isf} = 0.20 and V_{pc} = 0.55 ml/g.

To get closer to reality, the models have to be more complex. For example, the capillary wall is tiled with endothelial cells with transport occurring through interendothelial clefts and across the endothelial cell bodies, so PS_C actually represents a sum of two conductances in parallel, a transendothelial facilitated transport process and passive diffusion through the interendothelial cleft (Schwartz et al 2002); to account for this in the analysis the more complex model (of the

Table 3: Parameter Estimates at differing N_{tanks}

Species	N_{tanks} =	*15*	5	2	1
^{14}C-AraH	PS_c, ml g^{-1} min^{-1}	1.4	1.3	2.0	8.0
	PS_{pc}, ml g^{-1} min^{-1}	1.0	0.85	0.65	0.7
	V_{isf}, ml g^{-1}	0.33	0.3	0.28	0.2
	V_{pc}, ml g^{-1}	0.2	0.22	0.25	0.28
^{3}H-Adenosine	PS_c, ml g^{-1} min^{-1}	3	3	5	20
	PS_{pc}, ml g^{-1} min^{-1}	20	20	9	7
	V_{pc}, ml g^{-1}	0.55	0.55	0.55	0.55
	G_{pc}, ml g^{-1} min^{-1}	90	70	70	60

Footnote: No free parameters for fitting the Albumin curve. For the adenosine (Ado) analysis V_{pc} was fixed at 0.55 ml/g, and not optimized. All other parameters were estimated from the data.

form shown in Figure 10) is used to account separately for cleft permeation and transendothelial flux.

Discussion:

Metabolic events within cells are intimately linked with the external influences of substrate delivery and metabolite removal. These influences include the rates of transport by blood flow and transmembrane processes as well as the regulation of enzymatic reactions. Further influences include intravascular and intracellular binding, where one finds the influences discussed in Section I. An obvious example is that the transport of respiratory gases through the circulation is dominated by their binding and buffering in the blood, which in turn influence their rates of delivery and exchange. In Section I we showed that errors in parameterization occur when the assumption of instantaneous binding is incorrect to various degrees. A second inference is that parameter values obtained during steady state cannot be expected to have validity during a changing state, nor in a subsequent steady state where concentrations differ from those in the initial steady state.

Solute binding is common for pharmacologic agents, hormones, vitamins, and the body's normal constituents like fatty acids. In fact one can generalize by saying that most lipid soluble substances are carried in sequestered or bound form in the blood and that their fluxes into tissues and cells are facilitated by transporter proteins.

In Section II the emphasis is not merely a comparison of the efficacy of distributed versus compartmental models, but on the critical need to incorporate what is known about a system into the analysis. Accounting for the anatomy is as important as obeying conservation requirements. In general one needs to adhere to the constraints provided by prior studies, the anatomy being primary since it is usually well defined. Anatomy is accounted for by using PDEs in capillary-tissue exchange processes; failure to use anatomic information and to seek the simplicity of "minimal models" sacrifices the reality of estimates of the primary physiological parameters, particularly those like the permeability-surface area products, the membrane PSs, which dominate the kinetics: Single compartmental analysis gives estimates up to several-fold different from those emerging from high resolution analysis using the anatomic constraints. Qualitative compartmental

modeling is certainly useful for categorization or classification, and there are situations in which physical or physiological parameters are correctly estimated, given the veracity of the compartmental mixing assumption. This essay is an attempt to stimulate each modeler's curiosity and thoughtful assessment of the applicability of stirred tank aproximations.

ACKNOWLEDGEMENTS

Research supported NIH grants BE 001973, HL73598, and NSF grant 04-607/NIH. James Eric Lawson assisted with manuscript preparation. The models described here are available at http://www.physiome.org/models/.

REFERENCES:

10102. Bassingthwaighte JB, Yipintsoi T, and Harvey RB. Microvasculature of the dog left ventricular myocardium. Microvasc Res 7: 229-249, 1974.

10312. Bassingthwaighte JB, Wang CY, and Chan IS. Blood-tissue exchange via transport and transformation by endothelial cells. Circ Res 65: 997-1020, 1989.

10371. Bassingthwaighte JB, Chan IS, and Wang CY. Computationally efficient algorithms for capillary convection-permeation-diffusion models for blood-tissue exchange. Ann Biomed Eng 20: 687-725, 1992.

10573. Bassingthwaighte JB and Vinnakota KC. The computational integrated myocyte. A view into the virtual heart. In: Modeling in Cardiovascular Systems. Ann. New York Acad. Sci. 1015:, edited by S. Sideman and R. Beyar. 2004, p. 391-404.

10596. Bassingthwaighte JB, Raymond GR, Ploger JD, Schwartz LM, and Bukowski TR. GENTEX, a general multiscale model for [italic] in vivo [plain] tissue exchanges and intraorgan metabolism. Phil Trans Roy Soc A: Mathematical, Physical and Engineering Sciences 364(1843): 1423-1442, 2006.

7311. Beard DA, Liang S, and Qian H. Energy balance for analysis of complex metabolic netw orks. Biophys J 83: 79-86, 2002.

38. Berman M. The formulation and testing of models. Ann NY Acad Sci 108: 182-194, 1963.

87. Chinard FP, Vosburgh GJ, and Enns T. Transcapillary exchange of water and of other substances in certain organs of the dog. Am J Physiol 183: 221-234, 1955.

Cobelli C, Foster D, and Toffolo G. Tracer Kinetics in Biomedical research. From data to model. Kluwer Academic/Plenum Publishers, New York, 2000.

99. Crone C. The permeability of capillaries in various organs as determined by the use of the 'indicator diffusion' method. Acta Physiol Scand 58: 292-305, 1963.

Dash RK and Bassingthwaighte JB. Blood HbO2 and HbCO2 dissociation curves at varied O2, CO2, pH, 2,3-DPG and temperature levels. Ann Biomed Eng 32: 1676-1693, 2004.

Dash RK, Li Z, and Bassingthwaighte JB. Simultaneous blood-tissue exchange of oxygen, carbon dioxide, bicarbonate, and hydrogen ion. Ann Biomed Eng 34: 2006.

10234. Gorman MW, Bassingthwaighte JB, Olsson RA, and Sparks HV. Endothelial cell uptake of adenosine in canine skeletal muscle. Am J Physiol Heart Circ Physiol 250: H482-H489, 1986.

International Commission on Radiological Protection. Basic Anatomical and Physiological Data for Use in Radiological Protection: Reference Values. New York: Elsevier Science, 2003, 320 pp.

Kassab GS, Rider CA, Tang NJ, and Fung Y-CB. Morphometry of pig coronary arterial trees. Am J Physiol Heart Circ Physiol 265: H350-H365, 1993.

10233. Kuikka J, Levin M, and Bassingthwaighte JB. Multiple tracer dilution estimates of D- and 2-deoxy-D-glucose uptake by the heart. Am J Physiol Heart Circ Physiol 250: H29-H42, 1986.

320. Krogh A. The number and distribution of capillaries in muscles with calculations of the oxygen pressure head necessary for supplying the tissue. J Physiol (Lond) 52: 409-415, 1919.

10458. Li Z, Yipintsoi T, and Bassingthwaighte JB. Nonlinear model for capillary-tissue oxygen transport and metabolism. Ann Biomed Eng 25: 604-619, 1997.

10457. Poulain CA, Finlayson BA, and Bassingthwaighte JB. Efficient numerical methods for nonlinear facilitated transport and exchange in a blood-tissue exchange unit. Ann Biomed Eng 25: 547-564, 1997.

10529. Schwartz LM, Bukowski TR, Ploger JD, and Bassingthwaighte JB. Endothelial adenosine transporter characterization in perfused guinea pig hearts. Am J Physiol Heart Circ Physiol 279: H1502-H1511, 2000.

7931. Vinnakota K, Kemp ML, and Kushmerick MJ. Dynamics of muscle glycogenolysis modeled with pH time-course computation and pH dependent reaction equilibria and enzyme kinetics. Biophys J doi:10.1529/biophys.105.073296: 1-64, 2007.

10572. Vinnakota K and Bassingthwaighte JB. Myocardial density and composition: A basis for calculating intracellular metabolite concentrations. Am J Physiol Heart Circ Physiol 286: H1742-H1749, 2004.

10084. Yipintsoi T, Scanlon PD, and Bassingthwaighte JB. Density and water content of dog ventricular myocardium. Proc Soc Exp Biol Med 141: 1032-1035, 1972.